Near-IR Absorption and Photocurrent Generation Using a First-of-Its-Kind Boron Difluoride Formazanate Non-Fullerene Acceptor

(Supporting Information)

Josh D. B. Koenig[a], Mahmoud E. Farahat[a], Jasveer S. Dhindsa[b], Joe B. Gilroy*[b], and Gregory C. Welch*[a]

[a] Department of Chemistry, University of Calgary, Calgary, Alberta, Canada T2N 1N4.

[b] Department of Chemistry and the Centre for Advanced Materials and Biomaterials Research (CAMBR), The University of Western Ontario, London, ON, Canada N6A 5B7.

* Corresponding Authors:

Email: joe.gilroy@uwo.ca;
Phone Number: 1-519-661-2111 (ext. 81561)

Email: gregory.welch@ucalgary.ca;
Phone number: 1-403-210-7603

Keywords: organic photovoltaics, non-fullurene acceptor, BF_2 formazanate, perylene diimide, near-IR absorption

TABLE OF CONTENTS

1. Methods and Materials

Materials: FBT polymer donor: poly[(2,5-bis(2-hexyldecyloxy) phenylene)-alt-(5,6-difluoro-4,7-di(thiophen-2-yl)benzo[c][1,2,5]thiadiazole)] (PPDT2FBT) was purchased from Brilliant Matters. Fullerene acceptor [6,6]-phenyl-C_{61}-butyric acid methyl ester ($PC_{61}BM$) was purchased from Ossila. All other reactants, reagents, and catalysts were purchased from Millipore-Sigma or VWR and used without further purification.

CHN Elemental Analysis: Elemental analyses were performed by Johnson Li in the Chemical Instrumentation Facility at the University of Calgary (UofC). A Perkin Elmer 2400 Series II CHN Elemental Analyzer was used to obtain CHN data, using ~1.5 mg of sample (with particle sizes ranging between 0.2 and 0.5 mm in diameter).

Nuclear Magnetic Resonance (NMR): All NMR spectroscopy experiments were recorded using a Bruker Avance III 500 MHz spectrometer at the UofC. All experiments were performed in tetrachloroethane-d_2. Chemical shifts (referenced to residual solvent) were reported in parts per million (ppm). Multiplicities were reported as follows: singlet (s), doublets (d), triplets (t), quartet (q), doublet of doublets (dd), and multiplets (m).

High-resolution MALDI-TOF (HR MALDI-TOF): High-resolution MALDI-TOF mass spectrometry measurements were performed by Johnson Li in the Chemical Instrumentation Facility at the UofC. The sample solution (~ 1 µg/mL in dichloromethane) was mixed with matrix trans2-[3-(4-tert-Butylphenyl)-2-methyl-2-propenylidene]malononitrile (DCTB) solution (~5 mg/mL in methanol). All spectra were acquired using a Bruker Autoflex III Smartbeam MALDI-TOF, set to the positive reflective mode (Na:YAG 355 nm laser settings: laser offset = 62-69; laser frequency = 200 Hz; and number of shots = 300). The target used was Bruker MTP 384 ground steel plate target.

UV-Visible-NearIR Spectroscopy (UV-Vis-nIR): All absorption measurements were recorded in ambient conditions using Agilent Technologies Cary 60 optical spectrometer at the UofC. All solution UV-Vis-nIR spectra were measured with 2 mm quartz cuvettes, using $CHCl_3$ as solvent. Stock solutions (~1.0 mg/mL) of each compound were prepared, serially diluted to concentrations between 10^{-5} - 10^{-6} M, and then used to construct calibration curves for determining molar absorptivity. Neat films were prepared by spin-coating from a 1 % wt/v solution onto clean Corning glass slides. Prior to use, glass slides were cleaned with soap and water, acetone and isopropanol, and followed by UV/ozone treatment using a Novascan UV/ozone cleaning system.

Photoluminescence (PL): All emission measurements were recorded in ambient conditions using an Agilent Technologies Cary Eclipse fluorescence spectrophotometer at the UofC.

Atomic Force Microscopy (AFM): AFM measurements were performed by using a TT2-AFM (AFM Workshop) in tapping mode and WSxM software with an 0.01-0.025 Ohm/cm Sb (n) doped Si probe with a reflective back side aluminum coating at the UofC. Samples for AFM measurement were the same ones that were used to collect the respective the device parameters.

X-Ray Diffraction (XRD): All X-ray diffraction experiments were performed with a PROTO AXRD Benchtop Powder Diffractometer using θ-2θ scans and Cu K-α radiation at the UofC.

Cyclic Voltammetry (CV): Electrochemical measurements were performed using a CH Instruments Inc. Model 1200B Series Handheld Potentiostat. A standard 3-electrode setup was utilized, consisting of a freshly polished glassy carbon disk working electrode (WE), Pt-wire counter electrode (CE), and Ag-wire pseudo-reference electrode (RE). All measurements were referenced to the ferrocene/ferrocenium ($Fc^{+/0}$) redox couple as internal standard. All cyclic voltammetry experiments were performed at a scan rate of 100 mV/s. Sample solutions, with 1 mM compound and 0.1 M tetrabutylammonium hexafluorophosphate ($TBAPF_6$) supporting electrolyte, were prepared in anhydrous CH_2Cl_2. All electrochemical solutions were sparged with dry gas (either N_2 or argon) for 5 minutes to deoxygenate the system prior to measurements. The ionization potentials (IP) and electron affinities (EA) were estimated by correlating the 1st oxidation and 1st reduction potentials (E_p ox $Fc^{0/+}$, $E_{½}$ red $Fc^{0/+}$) to the normal hydrogen electrode (NHE), assuming the IP of $Fc^{0/+}$ to be 4.80 eV, respectively.[1]

Power Conversion Efficiency (PCE) and External Quantum Efficiency (EQE): The current density-voltage (J-V) curves were measured by a Keithley 2420 source measure unit. The photocurrent was measured under AM 1.5 illumination at 100 mW/cm^2 under a Solar Simulator (Newport 92251A-1000). The standard silicon solar cell (Newport 91150V) was used to calibrate light intensity. EQE was measured in a QEX7 Solar Cell Spectral Response/QE/IPCE Measurement System (PV Measurement, Model QEX7, USA) with an optical lens to focus the light into an area about 0.04 cm^2, smaller than the dot cell. The silicon photodiode was used to calibrate the EQE measurement system in the wavelength range from 300 to 1100 nm. All devices were tested at the UofC under ambient conditions.

Organic Photovoltaic (OPV) Devices: Inverted device architecture (ITO/ZnO/Ternary Active Layer/MoOx/Ag) was used in OPVs device fabrication. Devices were fabricated using ITO-coated glass substrates cleaned by sequentially ultra-sonicating with detergent and de-ionized water, acetone, and isopropanol followed by exposure to UV/ozone for 30 min. ZnO was subsequently deposited as a sol-gel precursor solution in a N_2 purge box following the method of Sun *et al.*[2] The ternary blend FBT: BF_2PDI_2: $PC_{61}BM$ was dissolved in dichlorobenzene at 1:1:0.5 weight ratio (total concentration of 10 mg/mL) and processed in air at room temperatures. The substrates with the cast active layers were kept in an N_2 atmosphere glovebox overnight before evaporating MoO_3 and Ag. The 10 nm of MoO_3 followed by 100 nm of Ag were thermally deposited under vacuum (10^{-5} Torr). Active areas of the devices were 0.14 cm^2.

Computational Details: Gas-phase B3LYP/6-31G(d,p) ground-state equilibrium geometry optimizations were considered within Gaussian 09.[3] To reduce the computational cost, all alkyl-substituents were truncated to methyl groups. Molecular dihedral angles were systematically altered to ensure that the optimized geometric lower energy minimum was not missed structure possessed no imaginary frequencies . The resulting structure was characterized through frequency calculations (at the same level of theory). TD-SCF calculations were also performed from this optimized geometry. Single point calculations were performed on this structure to generate molecular orbitals and electrostatic potential maps.

2. Synthetic/Experimental Procedures

Boron Difluoride Formazanate (EthylHexyl-N-annulated Perylene Diimide)$_2$ (BF_2PDI_2)

Starting materials 2,6-bis(4-ethynylphenyl)-4-phenyl-1-BF_2-formazanate (BF_2Ace_2) and ethylhexyl-N-annulated Perylene Diimide Bromide (Br-PDIN-EH) were prepared following known literature preparations.[4,5]

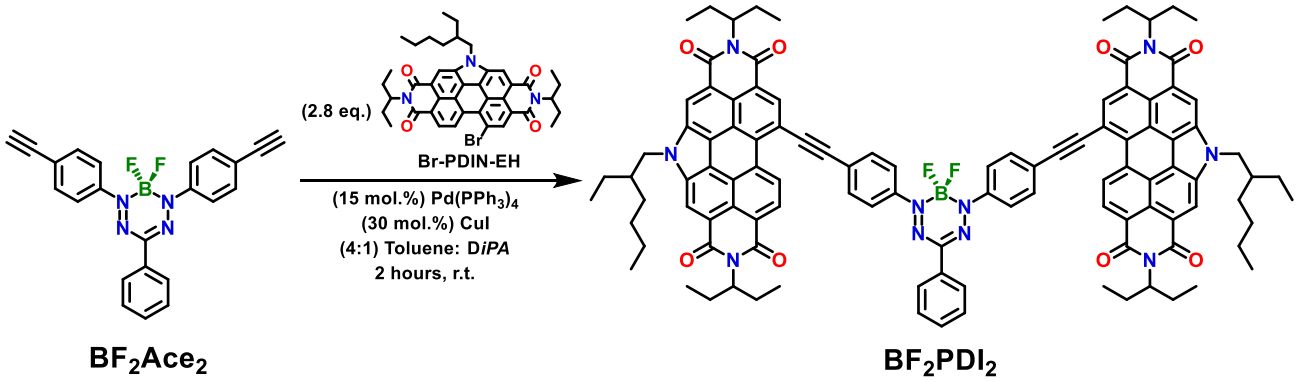

Br-PDIN-EH (103 mg, 0.14 mmol, 2.8 eq.), $BF_2(Ace)_2$ (19.9 mg, 0.05 mmol, 1.0 eq.), and CuI (2.8 mg, 0.015 mmol, 30 mol %) were combined into a 10 mL glass pressure vial. The vial was brought into the glovebox, $Pd(PPh_3)_4$ (8.7 mg, 0.008 mmol, 15 mol %) was added, and then the vial was sealed. A degassed mixture of toluene:diisopropylamine (4:1) was transferred into the vial using a Cannula line. The reaction mixture was stirred at room temperature for 2 hrs (monitoring reaction progress by TLC) and then subsequently quenched by pouring into H_2O (50 mL). The resulting solution was liquid-liquid extracted using CH_2Cl_2 (3 x 25 mL). The organic extracts were dried over Na_2SO_4 and then filtered through a short Celite plug. Organic solvent was removed by rotary evaporation and the resulting crude solid was purified by silica-gel column chromatography (eluting with CH_2Cl_2). The purified purple solid was precipitated into MeOH and collected by vacuum filtration (59 mg, 0.035 mmol, 69%).

^{1}H NMR (500 MHz, Tetrachloroethane-d_2) δ 9.67 (d, J = 8.3 Hz, 2H), 8.46 (s, 2H), 8.41 (s, 4H), 8.34 (d, J = 8.3 Hz, 2H), 7.58 (dd, J = 19.5, 7.6 Hz, 5H), 7.35 (d, J = 8.4 Hz, 4H), 6.99 – 6.88 (m, 4H), 4.59 – 4.51 (m, 4H), 4.15 (t, J = 8.1 Hz, 4H), 1.45 – 1.26 (m, 8H), 0.94 – 0.55 (m, 22H), 0.39 – 0.25 (m, 24H), 0.22 (t, J = 7.3 Hz, 6H).

^{13}C{^{1}H} NMR (126 MHz, Tetrachloroethane-d_2) δ 134.38, 132.01, 131.59, 130.82, 127.97, 126.06, 123.35, 122.97, 122.68, 121.37, 121.21, 119.03, 118.38, 118.23, 116.15, 109.40, 98.35, 78.70, 78.56, 78.48, 78.25, 73.03, 56.64, 40.27, 29.59, 27.35, 24.12, 23.03, 21.99, 12.99, 10.51, 10.50, 9.56. *quaternary centres were not observed due to limited solubility of BF_2PDI_2*

^{11}B NMR (161 MHz, Tetrachloroethane-d_2) δ -0.47 (t, $^1J_{BF}$ = 28.9 Hz, 1B).

^{19}F NMR (471 MHz, Tetrachloroethane-d_2) δ -143.24 (q, $^1J_{FB}$ = 28.4 Hz, 2F).

HRMS ([M-H]$^+$) calculated for M = $C_{107}H_{101}N_{10}O_8BF_2$: 1701.7786; detected [M-H]$^+$: 1701.7720.

CHN theoretical (%) C: 75.43, H: 5.98, N: 8.22; found (%) C: 74.74; H: 6.02; N: 7.94.

3. NMR Spectra

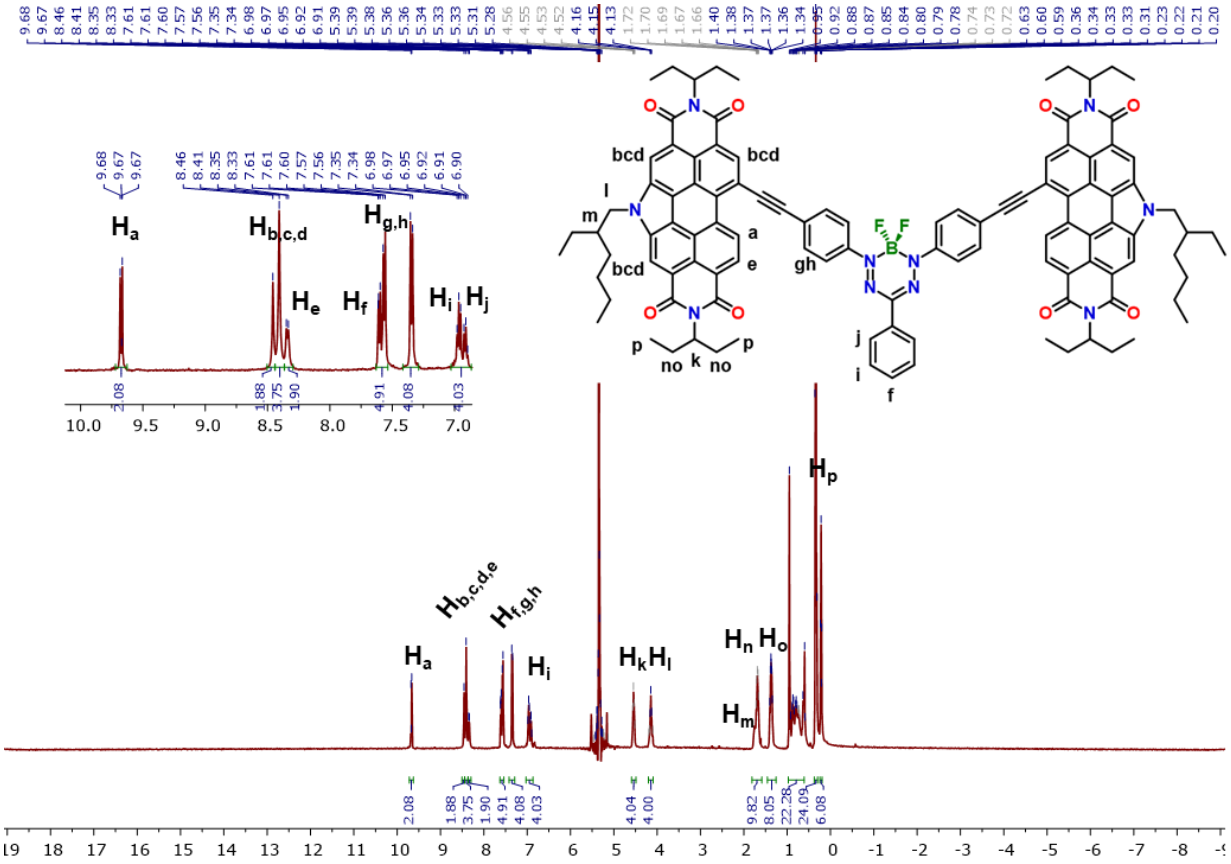

Fig. S1 ^{1}H NMR spectrum of BF_2PDI_2 (500 MHz, Tetrachloroethane-d_2).

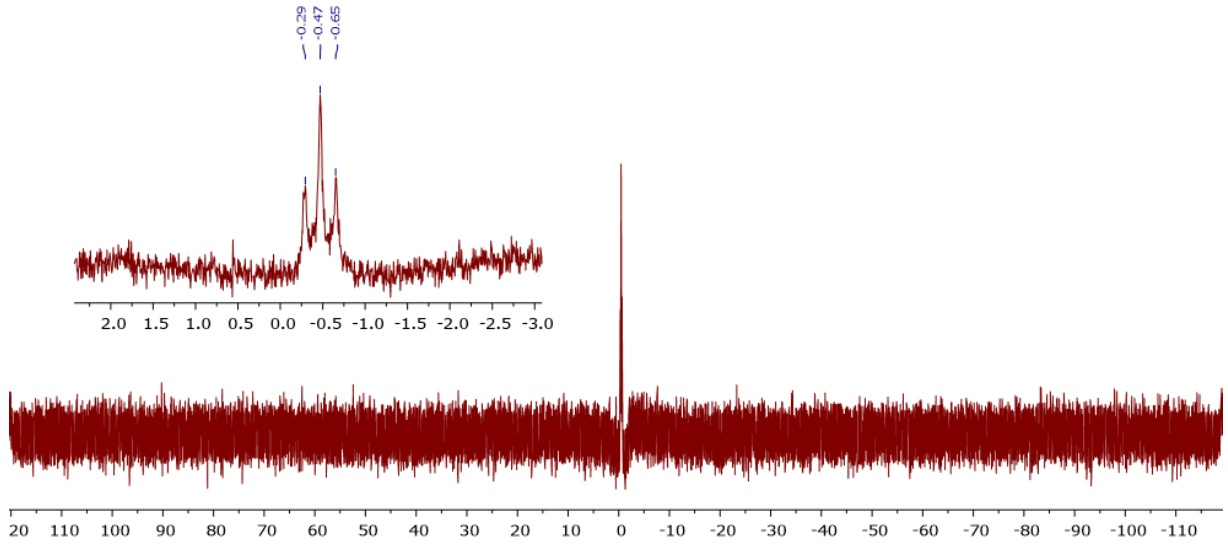

Fig. S2 ^{11}B NMR spectrum of BF_2PDI_2 (161 MHz, Tetrachloroethane-d_2).

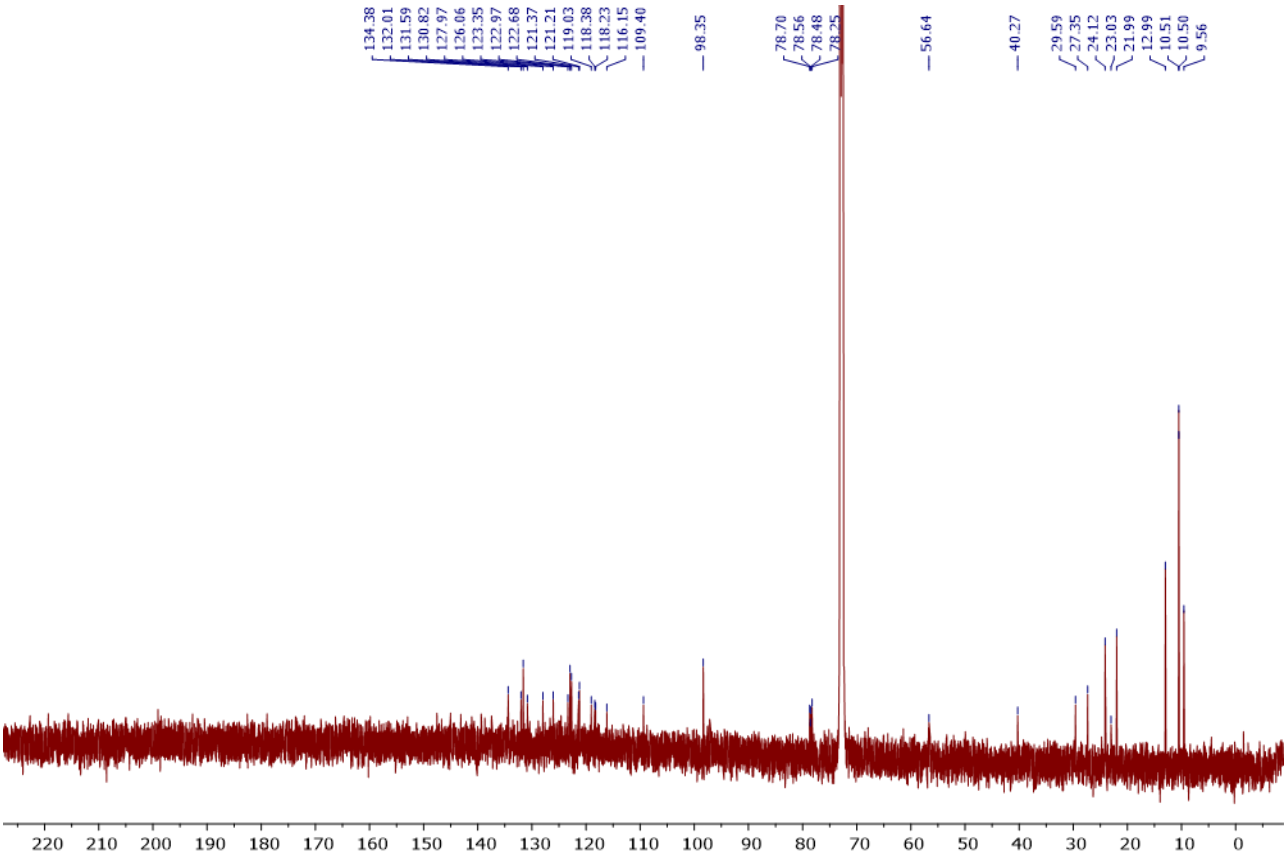

Fig. S3 $^{13}C\{^{1}H\}$ NMR spectrum of BF_2PDI_2 (126 MHz, Tetrachloroethane-d_2).

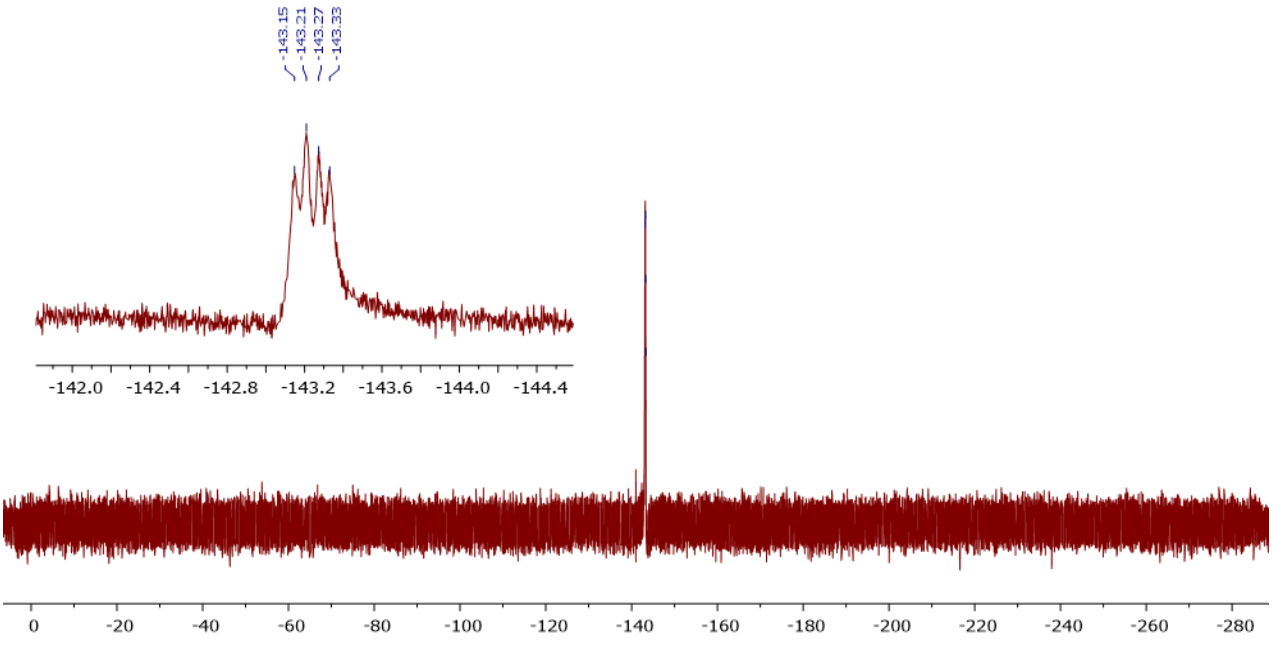

Fig. S4 ^{19}F NMR spectrum of BF_2 PDI_2 (471 MHz, Tetrachloroethane-d_2).

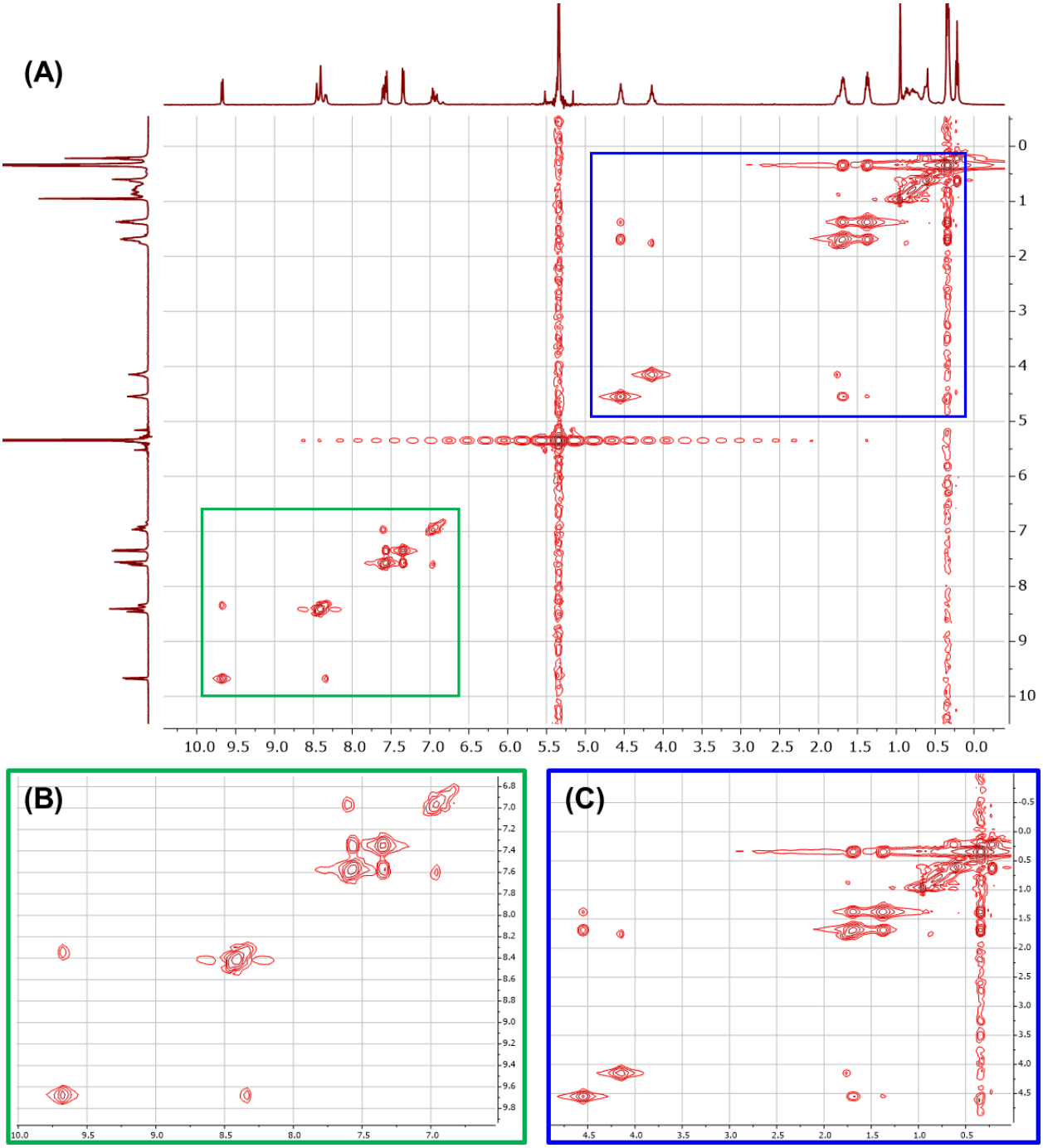

Fig. S5 ^{1}H-^{1}H COSY spectrum (A) of BF_2PDI_2 (500 MHz, Tetrachloroethane-d_2) with enhanced views of the aromatic (B) and aliphatic (C) regions.

4. MS, CHN EA, & Thermal Properties

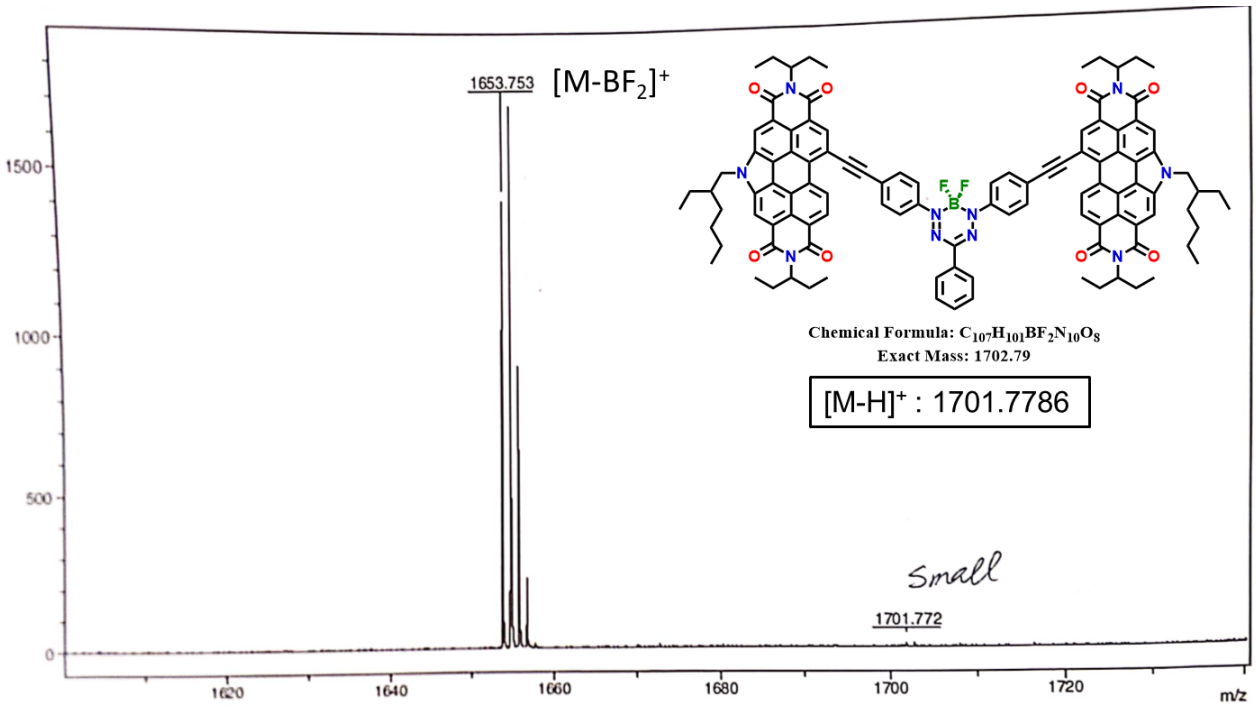

Fig. S6 HR MADLI TOF mass spectrum of BF_2PDI_2.

University of Calgary
Department of Chemistry EA Date: 2/5/2020

Name:	JOSH	Group:	GW
Sample:	BF_2PDI_2	Weight (mg):	1.59
%C (Actual):	74.74	%C (Theorectical):	75.43
%H (Actual):	6.02	%H (Theoretical):	5.98
%N (Actual):	7.94	%N (Theoretical):	8.22

Fig. S7 CHN elemental analysis of BF_2PDI_2.

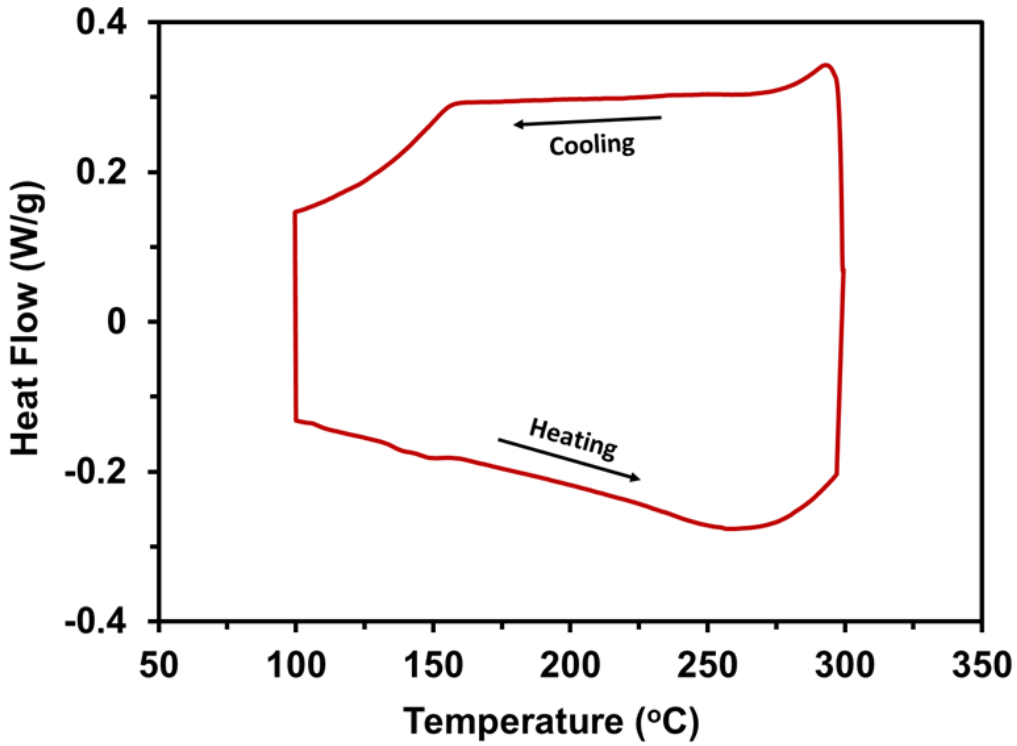

Fig. S8 Differential scanning calorimetry profile of BF_2PDI_2.

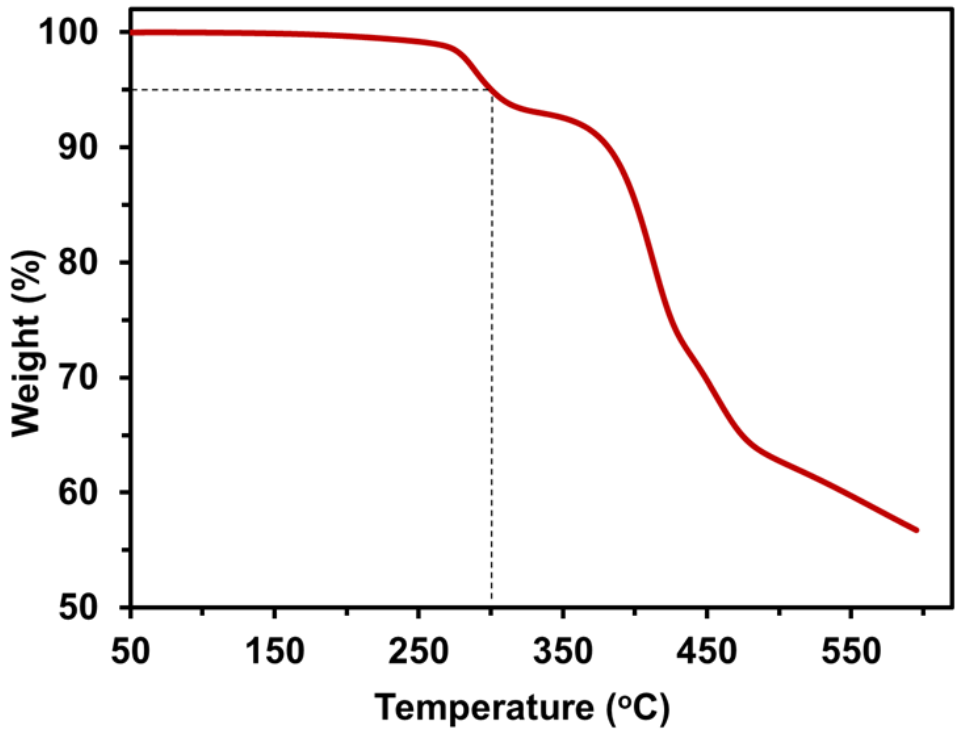

Fig. S9 Thermal gravimetric analysis profile of BF_2PDI_2.

5. UV-Visible Spectroscopy & Electrochemistry

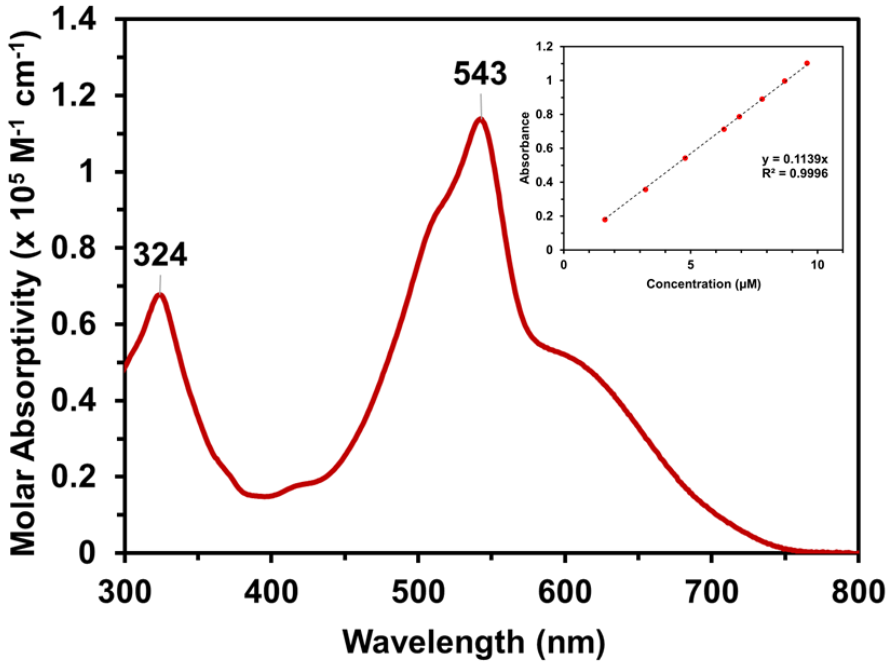

Fig. S10 UV-visible absorption spectrum of BF_2PDI_2 in $CHCl_3$, with calibration curve inset.

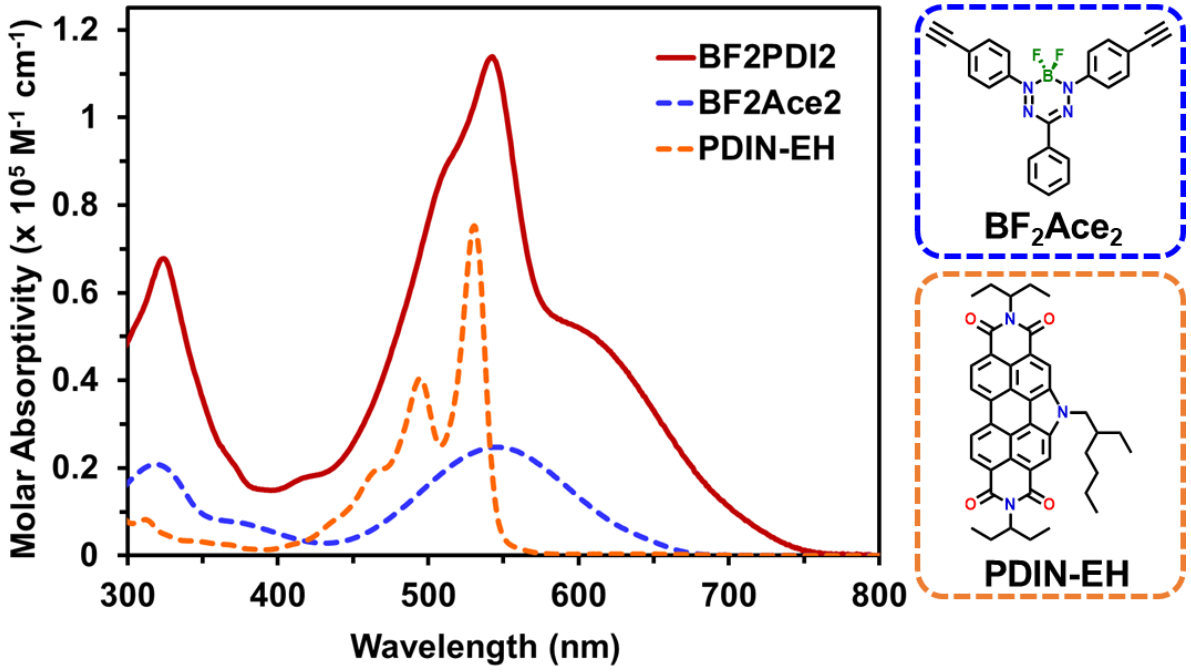

Fig. S11 Overlaid UV-visible absorption spectra of BF_2Ace_2, PDIN-EH, and BF_2PDI_2 in $CHCl_3$.

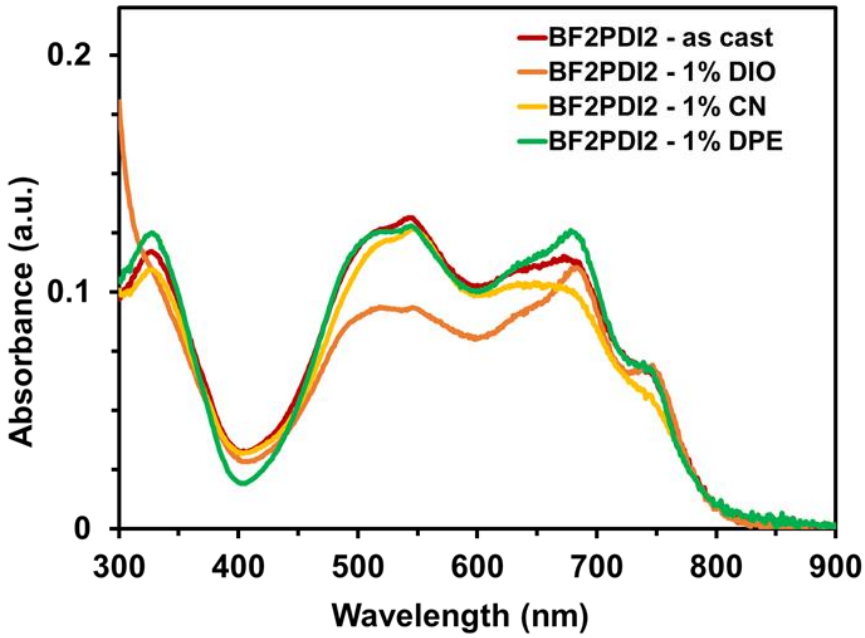

Fig. S12 Comparing the influence of solvent additives 1,8-diiodooctane (DIO), 1-chloronaphthalene (CN), and diphenyl ether (DPE) on the thin film UV-vis absorption spectra of BF_2PDI_2 (spin-coated from 10 mg/mL *o*-DCB solutions).

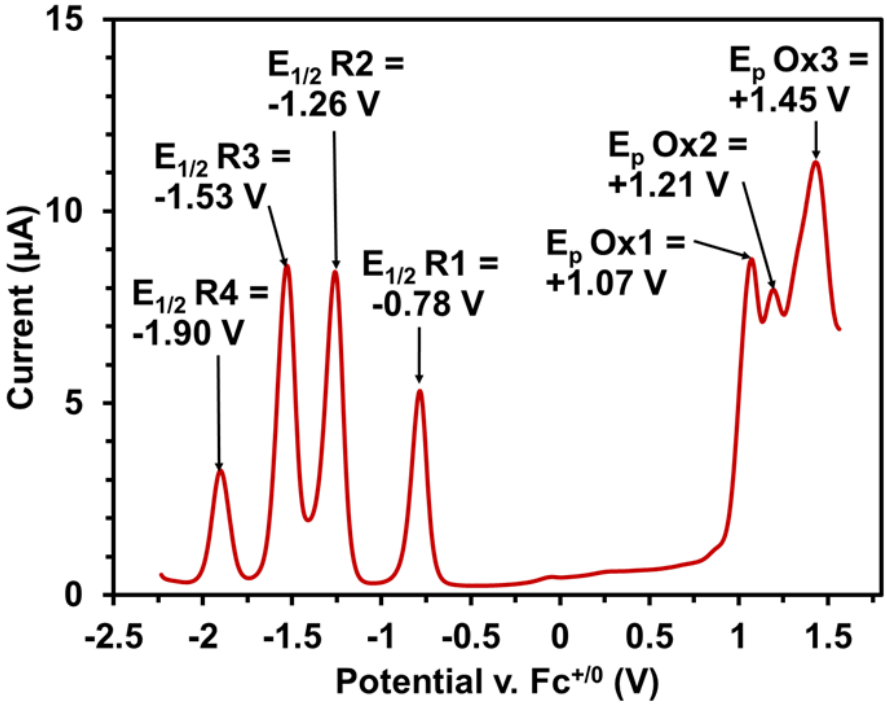

Fig. S13 Differential pulse voltammogram of BF_2PDI_2, measured in CH_2Cl_2 under argon with 0.1 M $TBAPF_6$ supporting electrolyte (WE = glassy carbon, CE = Pt-wire, *pseudo*-RE = Ag/AgCl).

6. Density Functional Theory

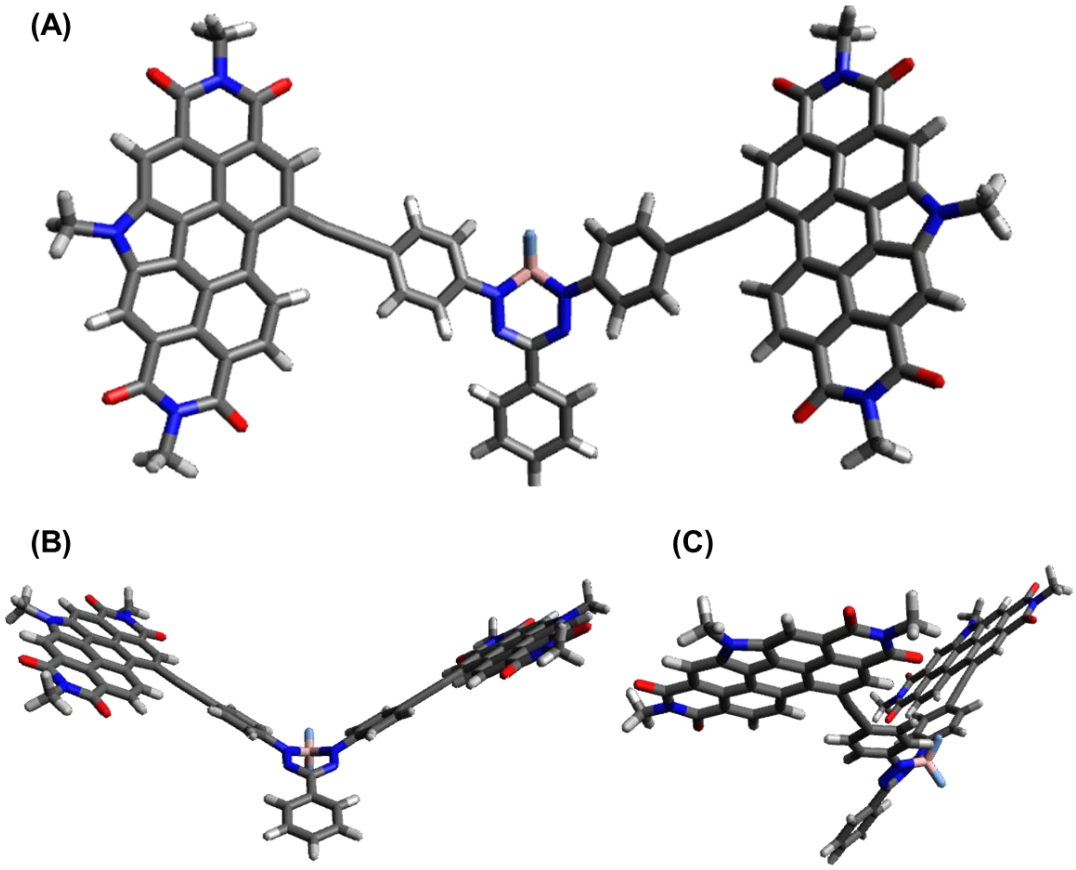

Fig. S14 Optimized geometry for BF_2PDI_2 at B3LYP/6-31G(d,p) ground-state.

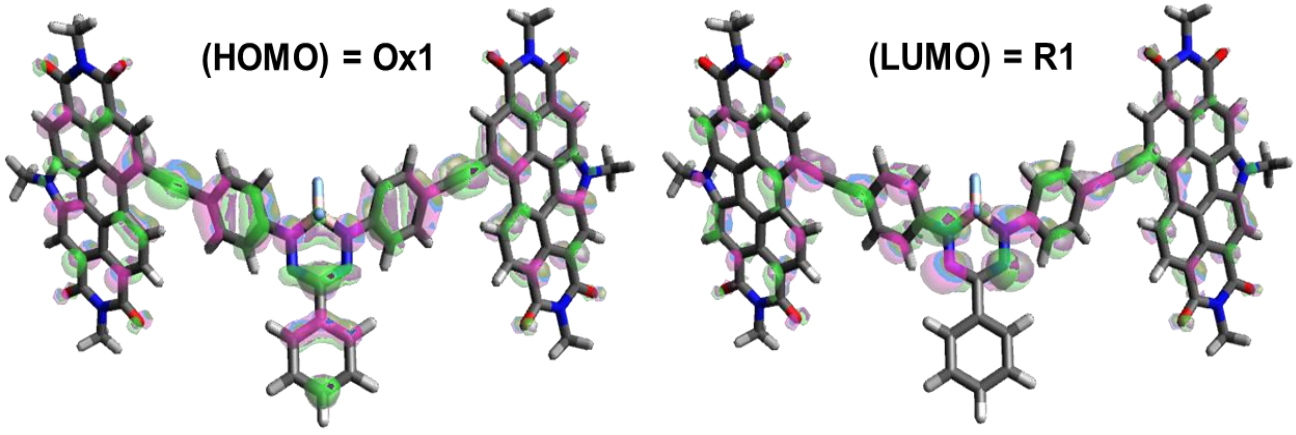

Fig. S15 Highest occupied molecular orbital (HOMO) and the lowest unoccupied molecular orbital (LUMO) for BF_2PDI_2 at B3LYP/6-31G(d,p) ground-state.

7. OPV Device Data

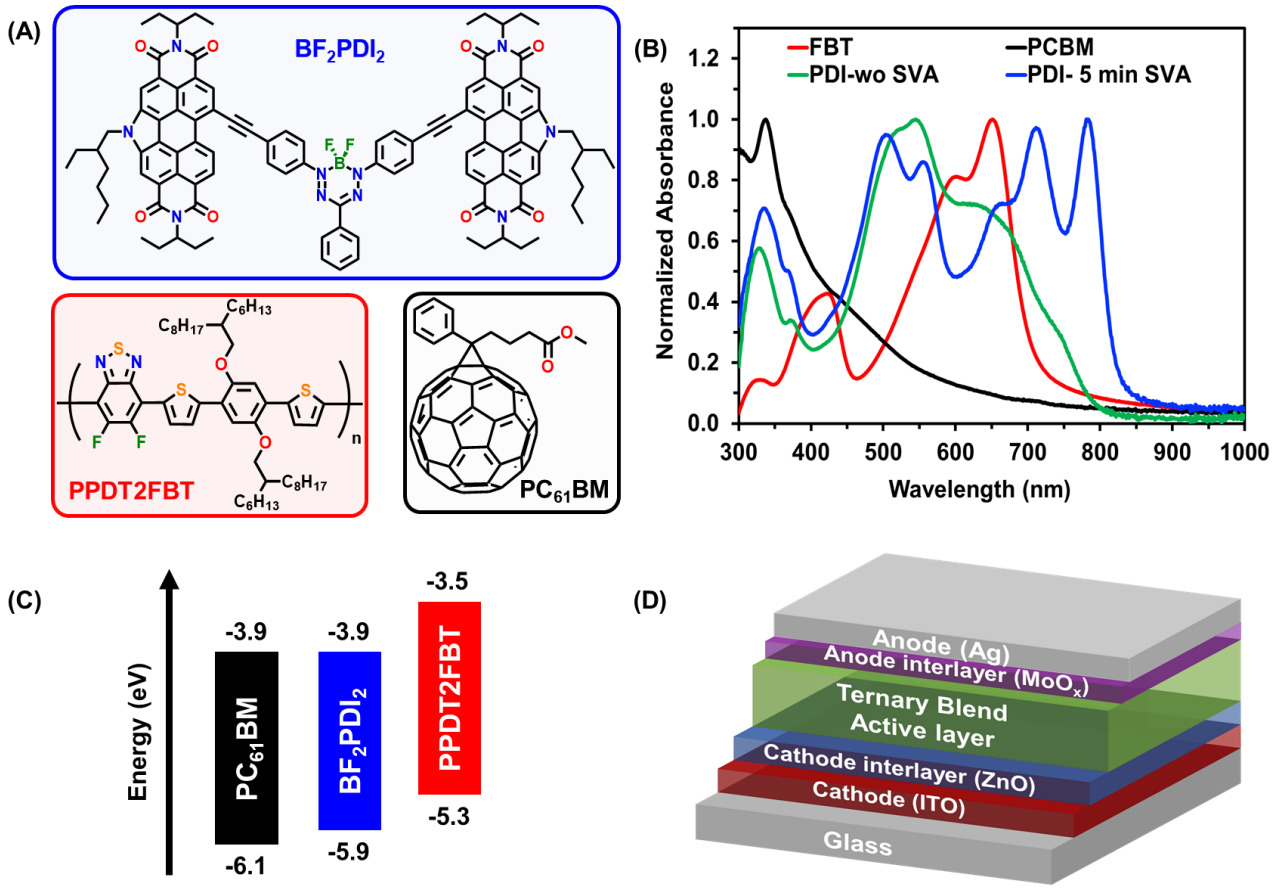

Fig. S16 Chemical structures (A), film optical absorption profiles (B), and energy levels (C) of all components used in the ternary blend active layer of the OPV (D). PDI = BF_2PDI_2, PCBM = $PC_{61}BM$, FBT = PPDT2FBT in the plot. SVA = solvent vapour annealing for 5 min using $CHCl_3$.

Table S1 Photovoltaic parameters of the devices based on ternary blend (PPDT2FBT: BF_2PDI_2: $PC_{61}BM$). Metrics in parenthesis correspond to the average values across 20 devices.

PPDT2FBT: BF_2PDI_2: $PC_{61}BM$	***V_{oc} (V)***	***J_{sc} (mA/cm^2)***	***FF (%)***	***PCE (%)***
As-cast (1:1:0.5, 10 mg/mL)	0.69 (0.69)	1.10 (1.02)	41.3 (40.1)	0.31 (0.28)
5 min SVA (1:1:0.5, 10 mg/mL)	0.64 (0.65)	1.95 (1.84)	48.6 (47.8)	0.61 (0.57)

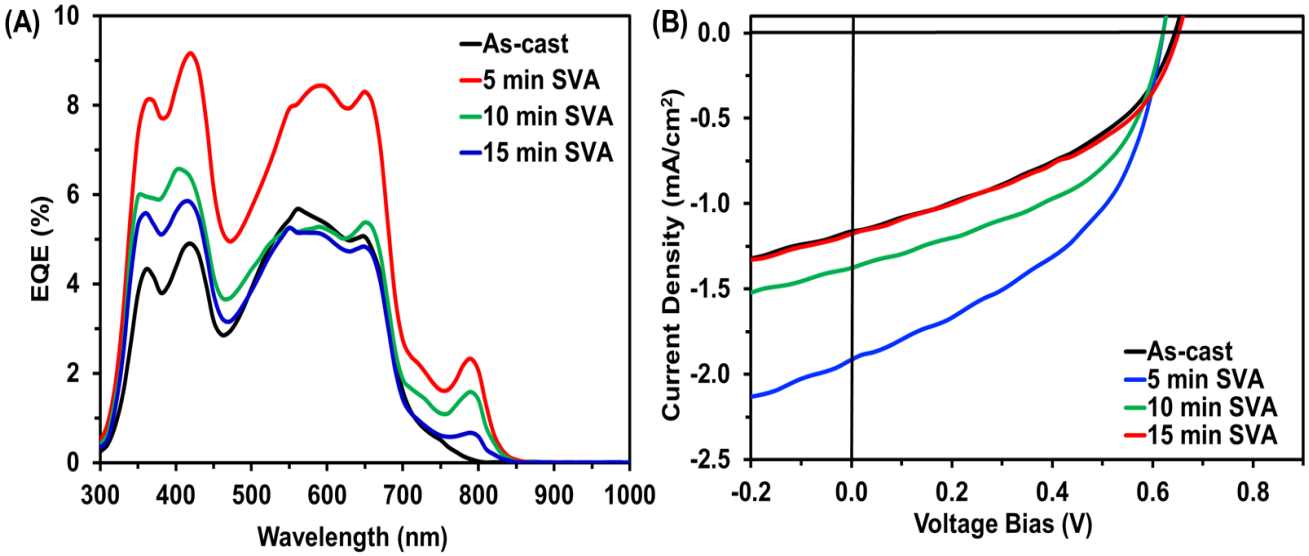

Fig. S17 External quantum efficiency plots (A) and J-V curves (B) comparing the effects of solvent vapor annealing duration on ternary blend OPV devices with PPDT2FBT: BF_2PDI_2: $PC_{61}BM$ (1:1:0.5) active layer at 10 mg/mL total concentration.

Table S2 Photovoltaic parameters of the devices based on ternary blend (PPDT2FBT: BF_2PDI_2: $PC_{61}BM$), comparing the effects of SVA treatment duration.

PPDT2FBT: BF_2PDI_2: $PC_{61}BM$	***V_{oc} (V)***	***J_{sc} (mA/cm^2)***	***FF (%)***	***PCE (%)***
As-cast (1:1:0.5, 10 mg/mL)	0.64	1.17	41	0.31
5 min SVA (1:1:0.5, 10 mg/mL)	0.62	1.91	45	0.53
10 min SVA (1:1:0.5, 10 mg/mL)	0.62	1.37	47	0.41
15 min SVA (1:1:0.5, 10 mg/mL)	0.65	1.18	41	0.32

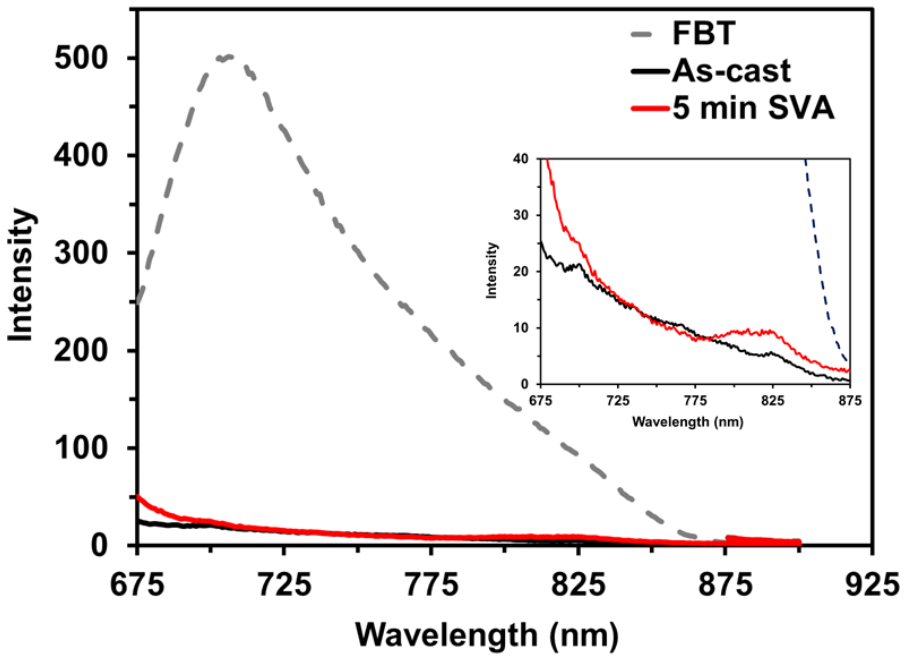

Fig. S18 Photoluminescence spectra of OPV devices with PPDT2FBT: BF_2PDI_2: $PC_{61}BM$ (1:1:0.5) active layer at 10 mg/mL total concentration, before (black) and after (red) solvent vapor annealing from $CHCl_3$. The excitation wavelength was 651 nm.

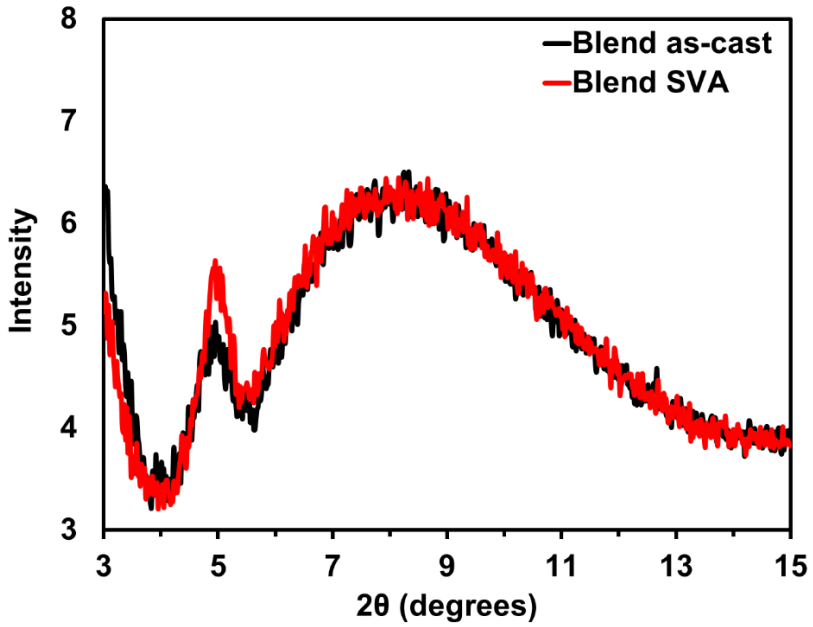

Fig. S19 X-ray diffraction spectra of spin-cast PPDT2FBT: BF_2PDI_2: $PC_{61}BM$ (1:1:0.5), before (black) and after (red) solvent vapor annealing from $CHCl_3$.

8. References

1 J. Pommerehne, H. Vestweber, W. Guss, R. F. Mahrt, H. Bässler, M. Porsch and J. Daub, Efficient Two Layer Leds on a Polymer Blend Basis, *Adv. Mat.*, 1995, **7**, 551–554.

2 Y. Sun, J. H. Seo, C. J. Takacs, J. Seifter and A. J. Heeger, Inverted Polymer Solar Cells Integrated with a Low-Temperature-Annealed Sol-Gel-Derived ZnO Film as an Electron Transport Layer, *Adv. Mat.*, 2011, **23**, 1679–1683.

3 M. Frisch, G. Trucks, H. Schlegel, G. Scuseria, M. Robb, J. Cheeseman, G. Scalmani, V. Barone, B. Mennucci, G. Petersson, H. Nakatsuji, M. Caricato, X. Li, H. Hratchian, A. Izmaylov, J. Bloino, G. Zheng, J. Sonnenberg, M. Hada, M. Ehara, K. Toyota, R. Fukuda, J. Hasegawa, M. Ishida, T. Nakajima, Y. Honda, O. Kitao, H. Nakai, T. Vreven, J. Montgomery, J. Peralta, F. Ogliaro, M. Bearpark, J. Heyd, E. Brothers, K. Kudin, V. Staroverov, R. Kobayashi, J. Normand, K. Raghavachari, A. Rendell, J. Burant, S. Iyengar, J. Tomasi, M. Cossi, N. Rega, J. Millam, M. Klene, J. Knox, J. Cross, V. Bakken, C. Adamo, J. Jaramillo, R. Gomperts, R. Stratmann, O. Yazyev, A. Austin, R. Cammi, C. Pomelli, J. Ochterski, R. Martin, K. Morokuma, V. Zakrzewski, G. Voth, P. Salvador, J. Dannenberg, S. Dapprich, A. Daniels, Farkas, J. Foresman, J. Ortiz, J. Cioslowski and D. Fox, *Gaussian 09 Revis*. E01 Gaussian Inc Wallingford CT.

4 S. M. Barbon and J. B. Gilroy, Boron Difluoride Formazanate Copolymers with 9,9-Di-n-Hexylfluorene Prepared by Copper-Catalyzed Alkyne–Azide Cycloaddition Chemistry, *Polym. Chem.*, 2016, **7**, 3589–3598.

5 A. D. Hendsbee, J.-P. Sun, W. K. Law, H. Yan, I. G. Hill, D. M. Spasyuk and G. C. Welch, Synthesis, Self-Assembly, and Solar Cell Performance of N-Annulated Perylene Diimide Non-Fullerene Acceptors, *Chem. Mater.*, 2016, **28**, 7098–7109.